


## Article

# Terrestrial Heat Flow and Lithospheric Thermal Structure of the Hubao Basin, North Central China

Ziqin Gong<sup>1</sup>, Wei Xu<sup>1,\*</sup> , Xiaoyin Tang<sup>2,\*</sup>, Genggeng Zhu<sup>3</sup>, Yuliang Yang<sup>1</sup>, Tianqi Guo<sup>1</sup> and Sen Wang<sup>1</sup>

<sup>1</sup> Institute of Global Environmental Change, Xi'an Jiaotong University, Xi'an 710049, China; 13212190552@163.com (Z.G.); 17751961385@163.com (Y.Y.)

<sup>2</sup> Institute of Geomechanics, Chinese Academy of Geological Sciences, Beijing 100081, China

<sup>3</sup> Exploration and Development Institute of PetroChina Changqing Oilfield Company, Yulin 718699, China; zgg1\_cq@petrochina.com.cn

\* Correspondence: xwsmpi@xjtu.edu.cn (W.X.); xyttang2019@126.com (X.T.)

**Abstract:** The terrestrial heat flow and lithospheric thermal structure of sedimentary basins are crucial for understanding basin dynamics and assessing geothermal resources. This study computed the heat flow in the Hubao Basin using rock thermal conductivity and borehole temperature data. Combined with the geophysical profile of the Yinshan Orogenic Belt–Hubao Basin–Ordos Basin, the lithospheric thermal structure was studied, and the geodynamic mechanism is discussed. The results indicate that the heat flow in the Hubao Basin ranges from 64.0 to 73.8 mW/m<sup>2</sup>. The Moho temperature along the profile varies between 570 and 652 °C, and the thickness of the thermal lithosphere ranges from 122.7 to 138.8 km. Using the backstripping method to calculate the crust–mantle heat flow ratio, we find that this ratio in the Hubao Basin is approximately 1, indicating a “warm crust, warm mantle” type of lithospheric thermal structure. This is related to the combined effects of extensional tectonics since the Late Jurassic and Early Cretaceous, westward subduction of the Pacific Plate, remote effects from the Indian Ocean Plate, and the development of deep-seated faults within the basin. The combined effects of lithospheric thinning and deep-seated faults have resulted in thermal anomalies in the Hubao Basin.

**Keywords:** Hubao Basin; heat flow; lithospheric thermal structure; mechanism analysis



**Citation:** Gong, Z.; Xu, W.; Tang, X.; Zhu, G.; Yang, Y.; Guo, T.; Wang, S. Terrestrial Heat Flow and Lithospheric Thermal Structure of the Hubao Basin, North Central China. *Water* **2024**, *16*, 1980. <https://doi.org/10.3390/w16141980>

Academic Editor: José Manuel Marques

Received: 12 June 2024  
Revised: 2 July 2024  
Accepted: 10 July 2024  
Published: 12 July 2024



**Copyright:** © 2024 by the authors. Licensee MDPI, Basel, Switzerland. This article is an open access article distributed under the terms and conditions of the Creative Commons Attribution (CC BY) license (<https://creativecommons.org/licenses/by/4.0/>).

## 1. Introduction

The heat flow and lithospheric thermal structure characteristics in sedimentary basins comprehensively reflect lithospheric tectonic-thermal evolution processes, which are crucial for studying basin dynamics and evaluating oil, gas, and geothermal resources [1]. The Hubao Basin is located in the southern part of the Yinshan Orogenic Belt in Inner Mongolia, forming a secondary basin within the Hetao tectonic belt. It is a Cenozoic faulted basin surrounded by the Yinshan Mountains to the north, the Lvliang Mountains to the east, and the Ordos Basin to the south (Figure 1). Due to the southward compression from the Central Asian Orogenic Belt to the north, northward compression from the North China Craton to the south, and the counterclockwise rotation of the Ordos Basin, the Hubao Basin exhibits complex topographic features with interlaced mountains and basins [2,3]. In the process of the interaction of the Eurasian plate, the (ancient) Pacific plate, and the Indian plate, the lithosphere in the study area has undergone drastic tectonic changes and the reconstruction of material and structure, and in-depth understanding of the thermal structure characteristics and lateral changes in this area will provide an important supplement for further research on the coupling relationship between sedimentary basins and orogenic belts. It is of great significance to understand the deep geodynamic process of the northern margin of North China Craton–Inner Mongolia fold belt and the dynamic mechanism of uplift of Yinshan Orogenic belt. In addition, geophysical exploration results, including gravity [4], electromagnetic methods [5], and seismic waves [6,7], indicate conditions conducive to high

heat flow in this region. In recent years, extensive exploration of geothermal resources has revealed that the northern part of the Hubao Basin harbors relatively abundant geothermal resources [8]. However, research on heat flow and lithospheric thermal structure in this area is sparse, and the formation mechanisms of heat sources remain unclear.

In this paper, we utilized borehole temperature data and geothermal gradient measurements from the Hubao Basin and its surrounding areas, combined with data on rock thermal conductivity, to study the distribution characteristics of heat flow in the region. Subsequently, based on the geophysical profile spanning the Yinshan Orogenic Belt–Hubao Basin–Ordos Basin [9,10], and integrating geological, structural, rock geochemical, and geophysical data, we established a mathematical model of the lithospheric structure profile. Using elevation, Bouguer gravity, geoid height, and heat flow as constraints, we applied the finite element method (Litmod-2D 2.0) [11] to determine the temperature distribution characteristics of the lithosphere and the lithospheric thermal structure of the Yinshan Orogenic Belt, Hubao Basin, and Ordos Basin; and the high thermal background of Hubao Basin, which are discussed and the deep geodynamic characteristics are revealed.

## 2. Geological Background

The Hohhot-Baotou Basin (hereinafter referred to as the Hubao Basin) is located in the Inner Mongolia Autonomous Region (Figure 1). It constitutes a narrow, east–west elongated Cenozoic fault basin in the Hetao region of Inner Mongolia [12]. Positioned at the northern margin of the North China Craton, adjacent to the Xingmeng Orogenic Belt, it lies at the boundary of two primary tectonic units [13]. During the Paleozoic and Mesozoic eras, it was primarily influenced by the Paleo-Asian Ocean tectonic system, the Late Paleozoic collision between the North China Craton and the Siberian Craton, and Mesozoic to present-day activities related to the Pacific Plate [14,15]. Due to recent tectonic activity, the Hubao Basin exhibits a dustpan-shaped structural feature, deep in the north and shallow in the south, with active faults at the mountain front being the main structures controlling sedimentation and evolution of the basin [16]. The basin is characterized by the continuous development of Cenozoic-Quaternary strata with immense thickness and significant lithological variations [17]. The Paleogene is dominated by fluvial-lacustrine deposits, mainly composed of brownish-gray and gray-green mudstone interbedded with fine sandstone and conglomerate. The Neogene is characterized by interbedded purple-brown and gray-green mudstone and fine sandstone, with localized occurrences of basalt. The Quaternary consists mainly of lacustrine deposits, characterized by yellow, gray-yellow, gray-green, and gray-black fine sand and clay interbedded with gravel. Due to the activity of frontal faults, Quaternary lacustrine sediments are exposed on the surface, discontinuously distributed along the piedmont terrace.

The Yinshan Orogenic Belt (YOB) is situated at the northern margin of the North China Craton and differs from typical plate margin subduction zones or collisional orogenic belts. It is a typical intracontinental orogenic belt [10]. Since the Middle-Late Jurassic to Cretaceous and continuing since the Neogene, left-lateral block movements have occurred due to the subduction of the eastern Pacific Plate and the collision of the Indian Plate with the Eurasian Plate, forming a series of rift zones [18]. With increasing elevation, Bouguer gravity anomalies rise, reaching up to  $-110$  mGal [4].

The Ordos Basin is a large Mesozoic intracontinental sag basin in the western part of the North China Craton, surrounded by fault basins on all sides [19]. It has undergone a long geological evolution from the Middle Paleozoic to the Tertiary, with thick sedimentary deposits averaging 4–5 km in thickness, and maximum thickness exceeding 10 km [20]. The basement consists of Precambrian and Paleozoic crystalline rocks and metamorphic rock sequences, overlain by Paleozoic, Mesozoic, and Cenozoic sedimentary strata [21]. The basin has extensively developed Silurian, Devonian, and Lower Carboniferous deposits; since the late Mesozoic, it has successively accumulated Triassic, Jurassic, Cretaceous, Tertiary, and Quaternary sediments [22]. The average crustal thickness of the Ordos Basin is approximately 42 km, with lithospheric thickness varying from 120 to 180 km from east

to west [23]. Internal deformation of the Ordos Basin is minimal, but due to its prominent movement compared to adjacent blocks, the surrounding graben basins are believed to result from mantle convection induced by the westward subduction of the Pacific Plate [7].

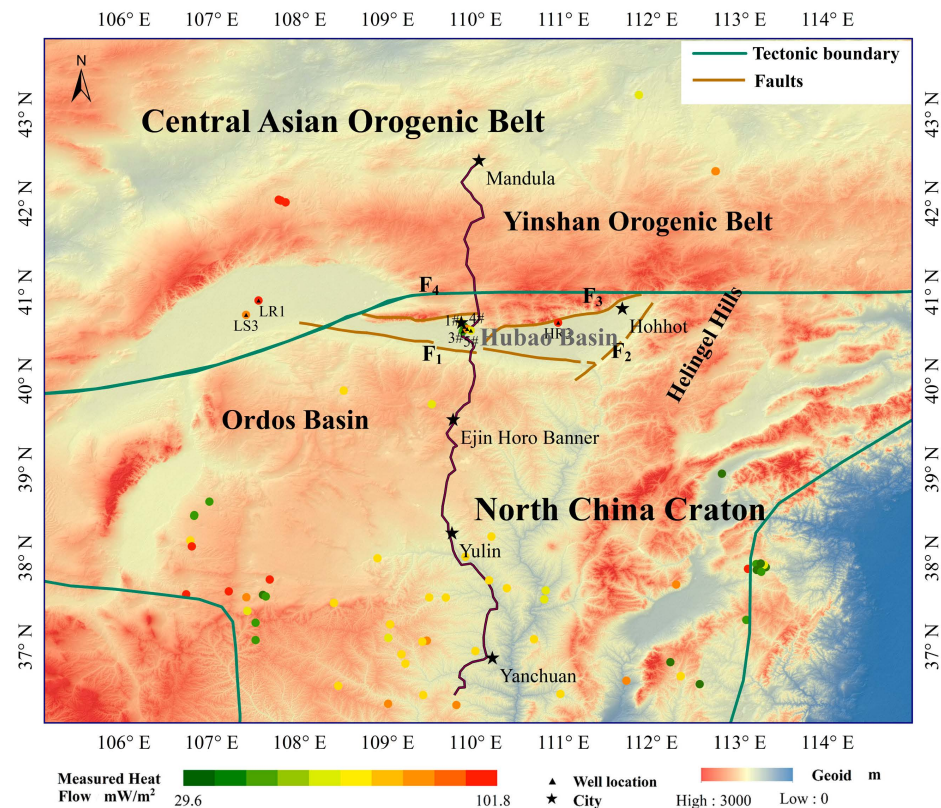


**Figure 1.** Regional geological map (the Yanchuan-Mandula Geophysical Profile was sourced from a shp file stored in ArcGIS, while the division of tectonic units is from Zhao et al. (2001) [24]. Elevation data were obtained from the Geospatial Data Cloud (<https://www.gscloud.cn/search>, 17 August 2023), and heat flow data were sourced from the Fourth Edition of the Chinese Heat Flow Database (<https://chfdb.xyz/>, 5 August 2023). The main faults were derived from “Peripheral Active Fault System of the Ordos” [25]. In the figure, F1 represents the northern margin fault of the Ordos Basin, F2 represents the Helingeer Fault, F3 represents the Daqing Mountain Frontal Fault, and F4 represents the southern margin frontal fault of the Ural Mountains.

### 3. Heat Flow

#### 3.1. Borehole Temperature and Geothermal Gradient

This study collected borehole temperature data from a total of eight wells in the Hubao Basin and surrounding areas (Figure 1), with depths ranging from 620 to 5500 m. The overall temperature increases with depth, exhibiting a conductivetype temperature curve (Figure 2), which is suitable for calculating terrestrial heat flow. The thermal conductivity data used in this study are shown in Table 1. Temperature data were regressed using the least squares method, and the slope of the fitted line numerically equals the corresponding temperature gradient. In this study, the GeothermoTool 1.0 software [26] was utilized to calculate the geothermal gradient, with specific values listed in Table 2. The results indicate that the distribution range of geothermal gradients in the study area is between 10.2 and 33.9 °C/km, with an average of  $24.9 \pm 5.7$  °C/km. Among these, well HR3 exhibits the highest geothermal gradient value at 33.9 °C/km, while well 3# shows the lowest geothermal gradient value at 10.2 °C/km. The geothermal gradient values of the remaining wells range from 18 to 30 °C/km.

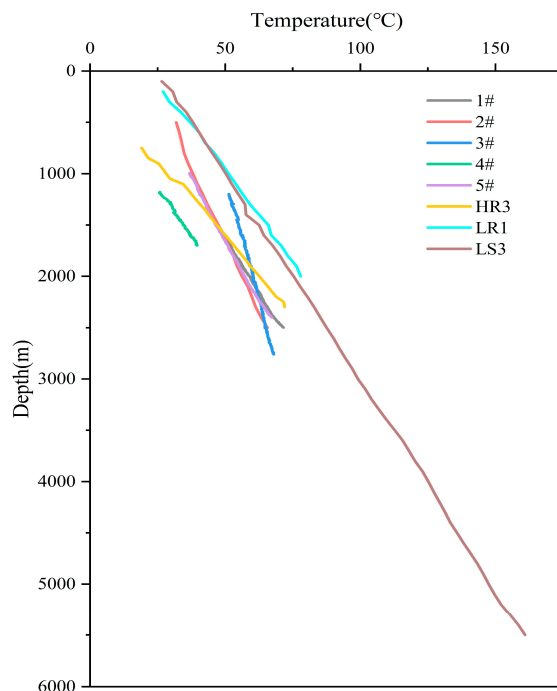


Figure 2. Temperature measurement curves of boreholes in the Hubao Basin and surrounding areas.

Table 1. Summary of sample information.

Geological Period	Number of Samples	Lithology	Thermal Conductivity (W/(m·K))
Neogene (N)	4	Sandstone, conglomerate, sandstone clay	2.67
Cretaceous (K)	4	Sandstone, mudstone, shale	1.83
Jurassic (J)	9	Sandstone, granite, feldspar quartz sandstone, limestone	2.75
Triassic (T)	2	Sandstone	4.96

Table 2. Calculation table of terrestrial heat flow value.

Well Number	Longitude	Latitude	Geothermal Gradient (°C/km)	Thermal Conductivity (W/(m·K))	Heat Flow (mW/m <sup>2</sup> )
1#	109.84°	40.66°	22.8	2.67	60.9
2# (ZK1)	109.86°	40.56°	18.9	2.67	50.5
3#	109.87°	40.61°	10.2	2.59	26.4
4#	109.90°	40.58°	26.7	2.55	68.1
5#	109.95°	40.56°	21.1	2.67	56.3
LR1	107.53°	40.90°	28.3	2.67	75.6
LS3	107.39°	40.74°	24.6	2.67	65.7
HR3	110.94°	40.65°	33.9	2.54	86.1

### 3.2. Thermal Conductivity

This study collected a total of 44 rock samples to measure thermal conductivity. Sampling points were located in key areas of Baotou City, Inner Mongolia, within the Hubao Basin, including Guyang County, Sha'erqin Village, and Dongsheng District. The collected samples encompass formations ranging from the Quaternary to the Precambrian, comprising lithologies such as limestone, sandstone, and metamorphic rocks. Due to the deep burial depth of some formations, the study primarily focused on formations from the Mesozoic to the Cenozoic. Thermal conductivity measurements were conducted using the Netzsch LFA447 thermal conductivity meter.

The thermal conductivity value ( $\lambda$ ) of each sample can be calculated using the following Formula (1), and the average value is obtained from two measurements for each sample:

$$K(T) = \alpha(T) \cdot C_p(T) \cdot \rho(T) \quad (1)$$

where  $K$  is thermal conductivity,  $W/(m \cdot K)$ ;  $\alpha$  is diffusivity,  $mm^2/s$ ;  $C_p$  is specific heat,  $J/g/K$ ;  $\rho$  is density,  $g/cm^3$ ; and  $T$  is temperature,  $^{\circ}C$ .

The thermal conductivity data from different wells were weighted by the proportional contribution of each geological layer, as indicated in Table 1. Through computation, the average thermal conductivity values were determined:  $2.67 W/(m \cdot K)$  for the Neogene,  $1.83 W/(m \cdot K)$  for the Cretaceous,  $2.75 W/(m \cdot K)$  for the Jurassic, and  $4.96 W/(m \cdot K)$  for the Triassic. The final average thermal conductivity obtained was  $3.05 W/(m \cdot K)$ .

### 3.3. Heat Flow

The heat flow value is calculated using the thermal conductivity and geothermal gradient values (Formula (2)).

$$Q = -K \frac{dT}{dZ} \quad (2)$$

where  $Q$  is the heat flow,  $mW/m^2$ ;  $K$  is the thermal conductivity,  $W/m \cdot K$ ; and  $\frac{dT}{dZ}$  is the geothermal gradient,  $^{\circ}C/km$ . The negative sign indicates that the heat flow direction is opposite to the direction of the geothermal gradient.

Based on measurements from eight wells and data from the Fourth Version Geothermal Database of the surrounding areas, a total of 125 sets of heat flow values were obtained. The spatial distribution of heat flow values in the region was interpolated using the Kriging method in ArcGIS 10.5 software, resulting in the characterization of the regional heat flow distribution (refer to Figure 3). The distribution of heat flow within the basin generally exhibits a trend of higher values in the west and lower values in the east. The overall heat flow values range from  $64.0$  to  $73.8 mW/m^2$ , with an average of  $65.7 \pm 14.7 mW/m^2$ . This average exceeds the mean heat flow value of  $60.4 \pm 12.3 mW/m^2$  reported in the Fourth Version Geothermal Database of mainland China [27]. However, it is lower than the heat flow values reported for the Bohai Bay Basin (approximately  $69 mW/m^2$ ) in eastern China [28] and the Songliao Basin (approximately  $76.9 mW/m^2$ ) [29].

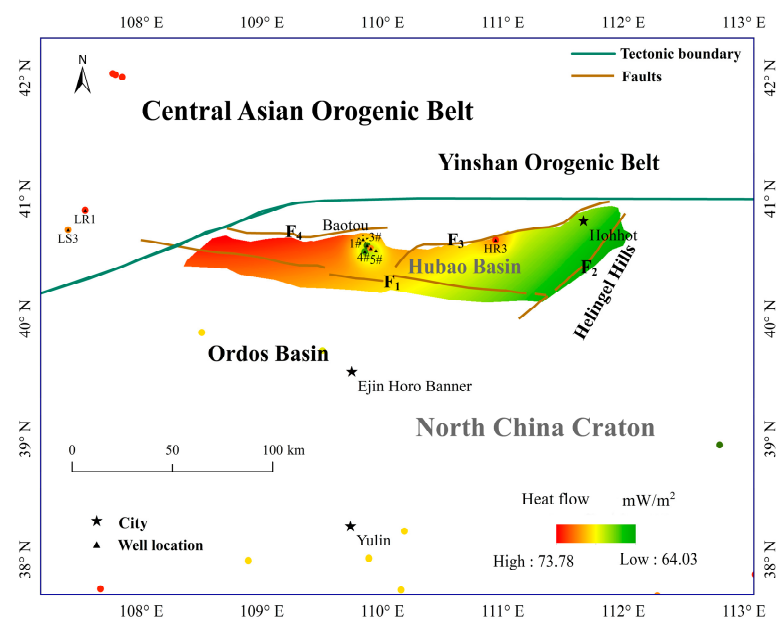


**Figure 3.** Terrestrial heat flow map of the Hubao Basin (different colored dots in the figure represent the heat flow value of that point).

## 4. Simulation of Lithospheric Thermal Structure

### 4.1. Methods and Data

#### 4.1.1. Methods

The main method employed in this study is the utilization of LitMod-2D 2.0 to simulate a profile spanning 670 km from the Yinshan orogenic belt to the Ordos Basin. LitMod-2D 2.0, developed by Afonso et al. (2008) [11], incorporates the LitMod finite element code to integrate petrological, mineral physics, and geophysical observational data within a consistent framework, enabling inference of lithospheric structure down to depths of 410 km. LitMod comprises FORTRAN subroutines based on the previous finite element code system CAGES architecture [30], partitioning the numerical domain into triangular elements representing different crustal and mantle bodies [11]. The 1330 °C isotherm was chosen to define the base of rigid and conductive layers [31], with temperature buffering applied in the lithosphere and asthenosphere regions to avoid unrealistic discontinuities in thermal gradients at the base of the lithosphere. Mineral assemblages in the upper mantle domain were computed using the Gibbs free energy minimization algorithm within the CaO-FeO-MgO-Al<sub>2</sub>O<sub>3</sub>-SiO<sub>2</sub> (CFMAS) system [32]. The physical properties of each mineral and blocky mantle, including density, thermal expansion coefficient, elastic parameters, and thermal conductivity, depend not only on temperature but also on pressure, composition, and phase transitions [33].

Crustal structure is inferred from seismic data, and the lithospheric structure in the study area was delineated into sedimentary layers, upper, middle, and lower crust layers. The model was constrained by importing elevation, Bouguer gravity, free-air gravity, geoid height, and heat flow data. Utilizing the finite element method, the steady-state heat conduction equation was solved, with boundary conditions set as follows: (1) constant surface temperature of 0 °C, (2) zero heat flow at lateral boundaries, and (3) fixed bottom temperature at 1330 °C [11]. Subsequently, the calculated values were compared with observed values to determine the optimal lithospheric structure model. This method, integrating data from petrology, mineral physics, and geophysics, enhances certainty compared to individual or paired modeling approaches.

#### 4.1.2. Data

This study is based on a profile traversing the Yinshan Orogenic Belt, the Hubao Basin, the Ordos Basin, and the Inner Mongolia Fold Belt, passing through Yan'an, Yulin, Ejin Horo Banner, Baotou, and finally reaching Mandula [34], with a total length of 670 km.

The heat flow data for the Hubao Basin primarily rely on deep temperature data collected from eight boreholes in the basin and surrounding areas, combined with measured rock thermal conductivity data to calculate the heat flow data for the Hubao Basin using Equation (2). The heat flow data for the Yinshan orogenic belt and the Ordos Basin mainly come from existing heat flow data, primarily sourced from the Chinese mainland heat flow database (Fourth Edition) [35], totaling 125 sets of heat flow values. The initial crustal layer structure used is primarily based on gravity measurement data from the Yanchuan–Baotou–Mandula geophysical profile [34] and deep seismic reflection data from the Hubao Basin in the Global Geosciences Transect Program [36].

The elevation data used in the profile was sourced from SRTMGL1 data: <https://lpdaac.usgs.gov/products/srtmgl1v003/> (15 September 2023); geoid height data were obtained from the geoid model provided by GMT [37]; Bouguer gravity data were derived from the WGM 2012 GLOBAL MODEL: <https://www.generic-mapping-tools.org/remote-datasets/earth-geoid.html> (1 September 2023); free-air gravity data were obtained from Pavlis et al. (2012) [37] and Sandwell et al. (2021) [38]. During the simulation process, the chemical composition of Baiyinzhu Rihe and gabbro distributed in the Baiyinzhu Rihe area of western Baiyun Ebo was utilized to generate mantle components [39]. A particle size of 5 mm and an elastic effect of 75 oscillation periods were selected as important parameters for generating the mantle [33].

### 4.1.3. Build Model

The initial crustal layer structure used in this study primarily relies on deep seismic reflection data [34] and the geological transect from Xiangshui to Mandula [36]. The crustal structure of the Yinshan Orogenic Belt–Hubao Basin–Ordos Basin is characterized by a layered structural system with varying thickness and burial depth distribution for each layer. Specifically, the upper crust ranges from 4.9 to 14.1 km in thickness, the middle crust ranges from 10.9 to 20.0 km, and the lower crust ranges from 9.2 to 22.8 km. The depth of the Moho interface varies between 35.4 and 43.8 km, while the thickness of the thermal lithosphere spans from 122.7 to 138.8 km. Notably, there are two major faults between the Hubao Basin and the Yinshan Orogenic Belt, as well as between the Yinshan Orogenic Belt and the Inner Mongolia Fold Belt, known as the Daqing Mountain Frontal Fault and the Ural Bao Lig Fault Zone (regionally known as the Baiyun Ebo Chifeng Fault), respectively. The Daqing Mountain Frontal Fault originated during the Eocene epoch, exhibiting intense activity during the Neogene period [40].

The profile is horizontally divided into four regions: the Ordos Basin, the Hubao Basin, the Yinshan Orogenic Belt, and the Inner Mongolia Fold Belt. Vertically, the lithosphere is divided into five parts: sedimentary layer, upper crust, middle crust, lower crust, and upper mantle. Each layer in each region has its corresponding parameters during the calculation process. Based on the established initial structural model, fundamental physical parameters are inputted. The data used for the sedimentary layer and the upper, middle, and lower crust are listed in Table 3. The thermal conductivity and heat production rates not referenced are based on measured values. The parameters for the upper mantle utilize the compositions of the lithospheric mantle components from Table 4, generated in LitMod-2D 2.0. Finally, the best-fit lithospheric structure model is obtained based on elevation, Bouguer gravity anomaly, geoid height, free-air gravity, and heat flow data (Figure 4). The thickness of the thermal lithosphere in the figure is referenced from previous studies [36,41,42].

**Table 3.** Stratified structure parameters of lithosphere strata.

Crustal Structure		Density (kg/m <sup>3</sup> )	Thermal Conductivity (W/(m·k))	Heat Production (μW/m <sup>3</sup> )
Sedimentary layer	1	2600 ①	2.74 ②	1.61 ②
	2	2490 ①	3.05	2.00
	3	2520 ①	3.05	2.00
	4	2620 ①	3.05	2.00
Upper crust	5	2710 ①	3.00 ③	1.67 ④
	6	2820 ①	3.00 ③	2.31 ⑤
	7	2820 ①	3.00 ③	2.31 ⑤
Middle crust	8	2920 ①	2.80 ③	0.83 ③
	9	2840 ①	2.80 ③	0.83 ③
Lower crust	10	3000 ①	2.60 ③	0.40 ③
Upper mantle	11	3245	2.10	0.03

① Wang et al. (2010) [34], ② Huang et al. (2015) [43], ③ Zang S (2013) [44], ④ Rao et al. (2016) [45], ⑤ Zuo et al. (2020) [46].

**Table 4.** Mantle composition table of the study area (wt%).

SiO <sub>2</sub>	Al <sub>2</sub> O <sub>3</sub>	FeO	CaO	MgO	K <sub>2</sub> O	Na <sub>2</sub> O
52.26	17.62	5.0	12.05	7.25	0.28	1.81

## 4.2. The Thermal Structure of the Lithosphere

### 4.2.1. The Deep Temperature of the Lithosphere

By comparing the fitted values with the measured values, adjustments were made to obtain the final fitted and measured value plot (Figure 5). The crustal fitting results are generally consistent with previous studies, with the overall crustal thickness consistent

with prior research. The Moho depth ranges from 35.4 to 43.8 km, and the lithospheric thickness spans from 122.7 to 138.8 km. The study indicates that elevation, Bouguer gravity anomaly, geoid height, free air anomaly, and heat flow demonstrate good fitting effects and can reflect actual information values. Some deviations between fitted values and measured values were observed, which may be attributed to model stratification, mantle composition, and density variations between different regions. Finally, deep temperature distribution data can be obtained (Figure 6). The results reveal that the Moho temperature ranges from 570 to 652 °C along the geophysical profile, with lower Moho temperatures observed in the Hubao Basin, reaching a minimum of 570 °C.

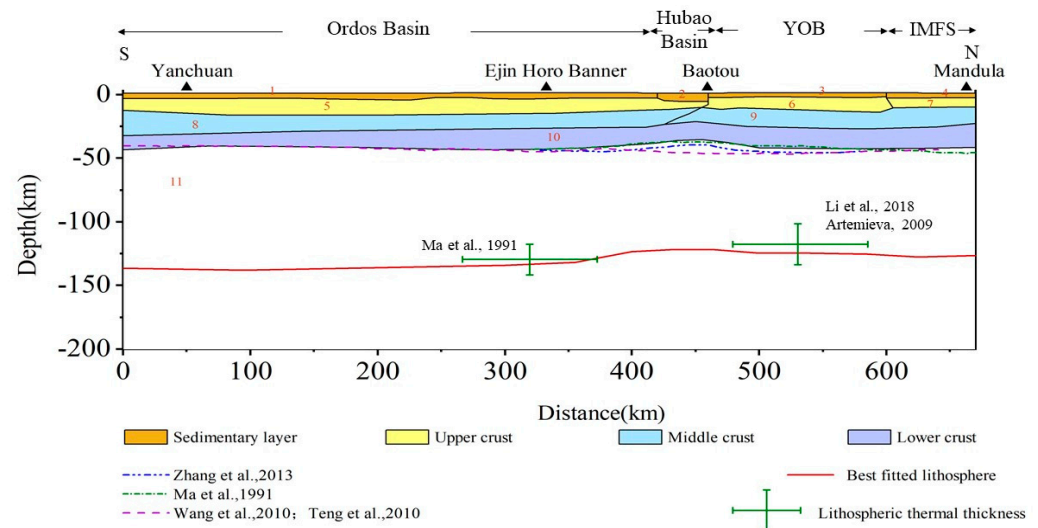


**Figure 4.** Stratified structure of the lithosphere in the geological section of Yinshan Orogenic Belt-Hubao Basin-Ordos Basin (IMFS = Inner Mongolia Fold System). ① Zhang et al. (2013) [15], ② Ma et al. (1991) [36], ③ Wang et al. (2010) [34], ④ Teng et al. (2010) [9], ⑤ Li et al. (2018) [41], ⑥ Artemieva et al. (2009) [42].

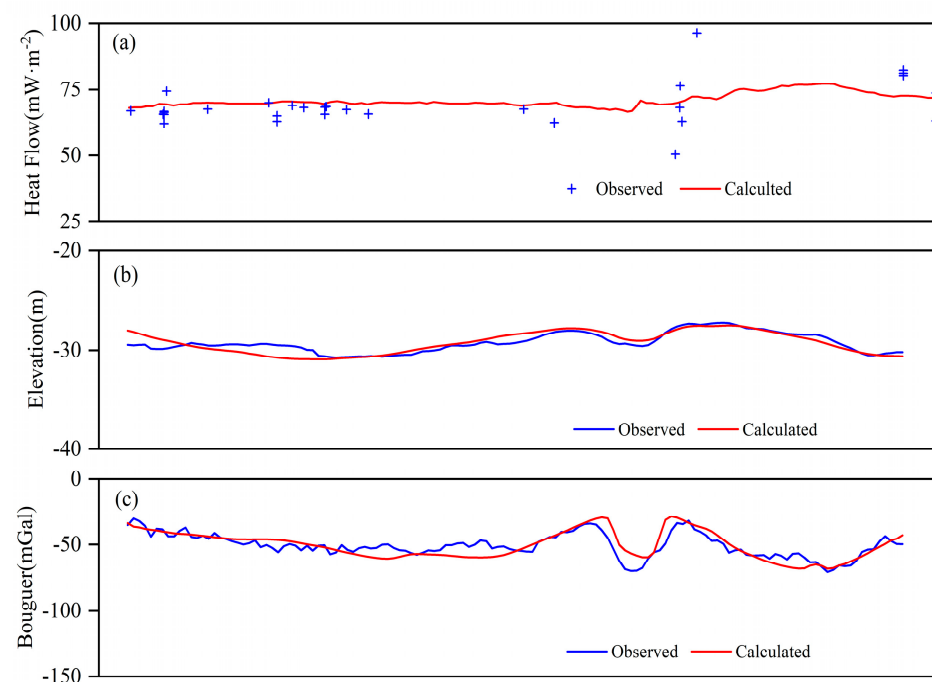


**Figure 5.** Cont.



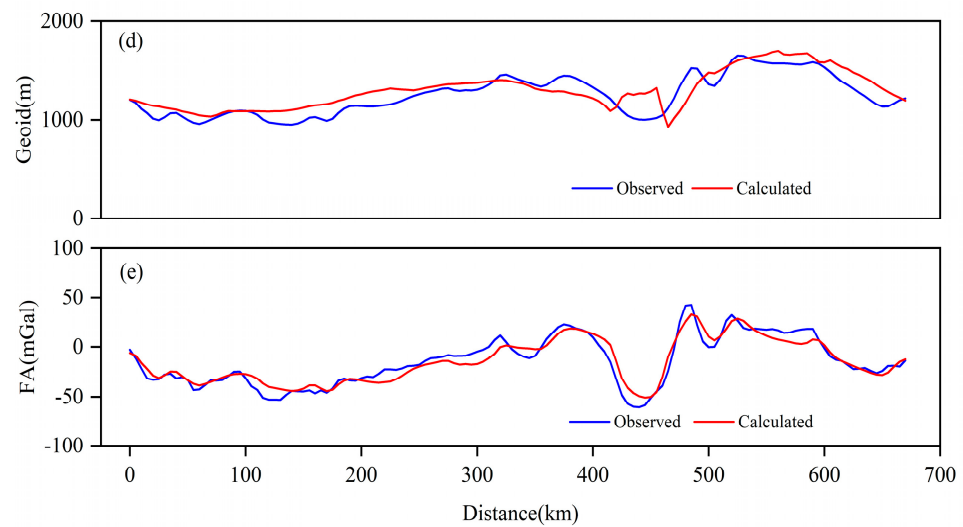


**Figure 5.** Simulation results of the Yinshan Orogenic Belt-Hubao Basin-Ordos Basin. (a) Heat flow; (b) elevation; (c) Bouguer gravity; (d) geoid; (e) free air.

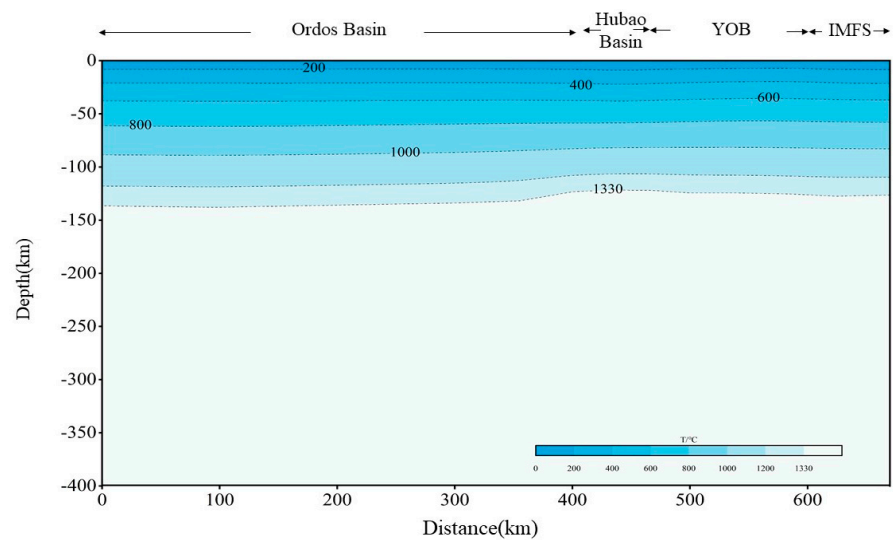


**Figure 6.** Deep temperature map of Yinshan Orogenic Belt-Hubao Basin-Ordos Basin profile.

#### 4.2.2. Lithospheric Thermal Thickness

In this study, the 1330 °C isotherm was adopted as the lower boundary temperature of the thermal lithospheric layer. By considering the characteristics of the lithospheric temperature distribution, the thickness of the thermal lithospheric layer was determined, ranging from 122.7 to 138.8 km. The distribution of thermal lithospheric layer thickness along the geophysical profile in the study area exhibits non-uniformity. From the Ordos Basin to the Hubao Basin and then to the Inner Mongolia Fold System, it displays a pattern of thick–thin–thick variations. The thickness of the thermal lithospheric layer in the Ordos Basin fluctuates within the range of 123.3 to 138.8 km, while in the Hubao Basin, it ranges from 122.7 to 123.3 km, with an average value of  $122.9 \pm 0.21$  km, making it the thinnest region of the thermal lithospheric layer along the profile. Within the Yinshan Orogenic Belt, the thickness of the thermal lithospheric layer spans from 122.9 to 127.0 km, and in the Inner Mongolia Fold System, it ranges from 127.2 to 128.9 km.

#### 4.2.3. The Distribution of Heat Flow between the Lithospheric Crust and Mantle

Based on the above simulations, a thermal flow profile spanning the Hubao Basin was obtained. The heat flow of geophysical cross-sections shows a trend of low in the south and

high in the north, indicating the existence of heat flow anomalies in the Hubao Basin and northern regions. The observed surface heat flow is mainly composed of two parts: one is the heat released by the radioactive decay of U, Th, and K in the shallow crust, and the other is the heat from the deep mantle [1]. The proportion and relationship between these two parts are the main content of studying the thermal structure of continental regions [47,48]. Using the backstripping method, the crust–mantle heat flow ratio of the calculated tectonic units can be obtained.

To determine the contributions of the crust and mantle to the terrestrial heat flow, an analysis of lithospheric thermal structure was conducted.

$$q = q_m + q_c = q_m + A_i Z_i \quad (3)$$

$$A_i = A_0 \exp(-z/D_i) \quad (4)$$

In the equation,  $q$  represents the surface heat flow,  $q_m$  denotes the heat flow from the deep mantle, and  $q_c$  stands for the contribution of radioactive decay of elements in the crust.  $A_i$  represents the heat production rate (in  $\mu\text{W}/\text{m}^3$ ) of each layer, while  $A_0$  is the surface heat production rate (in  $\mu\text{W}/\text{m}^3$ ), obtained from measured heat production rates in the sedimentary layer in this study.  $D$  represents the thickness (in kilometers) of the radioactive element-enriched layer, and a value of 10 km is chosen for  $D$  in this paper.

The crustal heat flow can be calculated by multiplying the thickness  $Z_i$  (in kilometers) of each crustal layer by its corresponding heat production rate  $A_i$ . Based on the simulated lithospheric structure, the thicknesses of the upper, middle, and lower crust can be obtained. The heat production rate for the sedimentary layer comes from measured data, while for the upper, middle, and lower crust, the heat production rate data are calculated according to the exponential model proposed by Lachenbrych (Formula (4)). With Formula (3), a layered model for the Hubao Basin can be derived (refer to Figure 7).

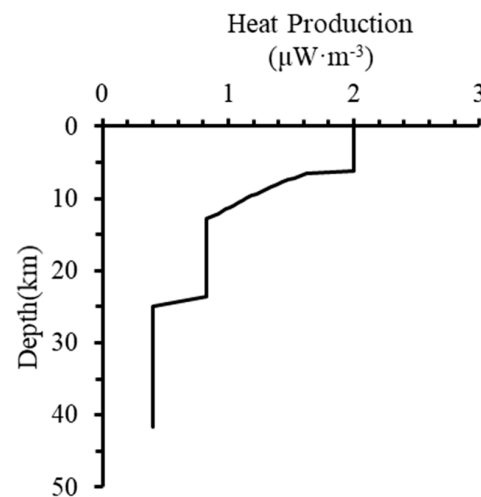


**Figure 7.** Crustal stratification model of the Hubao Basin.

Based on the above analysis, the calculated stratified heat flow for the Hubao Basin yields approximately  $36.5 \text{ mW}/\text{m}^2$  for crustal heat flow and approximately  $33.3 \text{ mW}/\text{m}^2$  for mantle heat flow, resulting in a crust–mantle heat flow ratio of approximately 1.1. The mantle heat flow is an important parameter reflecting the deep thermal state. In tectonically active areas, such as the eastern Bohai Bay Basin, the average mantle heat flow is around  $30\text{--}45 \text{ mW}/\text{m}^2$  [49]. In tectonically stable areas, such as the western Tarim Basin, the mantle heat flow ranges from  $6$  to  $15 \text{ mW}/\text{m}^2$  [50]. The crust–mantle heat flow ratio close to 1 in the Hubao Basin indicates that the mantle heat flow from the deep Earth is approximately equal to the radiogenic heat contribution from the crustal rocks. Thus, the basin exhibits a “warm crust, warm mantle” type of lithospheric thermal structure.

## 5. Analysis of the Heat Source Formation Mechanism in the Hubao Basin

The research results indicate that the Hubao Basin exhibits relatively high heat flow values ranging from  $64.0 \pm 73.8 \text{ mW/m}^2$ , with an average of  $65.7 \pm 14.7 \text{ mW/m}^2$ . The crustal heat flow is approximately  $36.5 \text{ mW/m}^2$ , while the mantle heat flow value is  $33.3 \text{ mW/m}^2$ . The crust–mantle heat flow ratio in the basin is approximately 1.1, indicating a “warm crust, warm mantle” type of thermal structure. The crustal thickness in the Hubao Basin is relatively thin, with an average of about 36.1 km, and the crustal temperature varies significantly between 570 and 593 °C. The average thickness of the thermal lithosphere is approximately 122.9 km, which is less than that of the southern Ordos Basin. Factors contributing to the thermal anomaly in this region primarily stem from the radioactive heat generation in the crust and the transfer of heat from the deep mantle.

The value of crustal heat flow primarily depends on the thickness of each layer in the crust and the abundance of radioactive elements within it. Previous studies have indicated that the Baiyun Ebo mining area in the northern part of the Hubao Basin is rich in U and Th [51,52], with Th content significantly exceeding the crustal Clark value [53]. Furthermore, soil samples from the Hubao Basin have shown enrichment in U and Th [54], confirming the presence of radioactive elements within the basin’s sediment. Uranium deposits in the Hubao Basin are commonly found within Cretaceous, Jurassic, Proterozoic, and Archean strata. The concentration of radioactive nuclides, such as uranium, thorium, and potassium, in intrusive rocks within the area tends to increase from older to younger formations and from basic to neutral to acidic rocks. Particularly high concentrations of potassium, uranium, and thorium are observed in Yanshanian, Indosinian, and Late Variscan granites, serving as significant uranium sources for Mesozoic and Cenozoic basins within the region [55].

The Hubao Basin, situated on the northern periphery of the North China Craton, is underlain by early Cambrian metamorphic rocks. It has experienced multiple stages of metamorphism and deformation, evolving from a Jurassic sedimentary basin during the Yanshanian period, influenced by changes in the main stress direction of the North China block [9]. The lithospheric structure of the Hubao Basin reflects a state of thinning, attributed to the combined effects of extensional tectonics since the Late Jurassic and Early Cretaceous, along with the westward subduction of the Pacific Plate and the distal influence of the Indian Ocean Plate. Subduction of the Pacific Plate, potentially stalled within the transition zone of the East Asian lower mantle, might generate a substantial mantle wedge in the upper mantle [56,57]. Angular flow and deep plate dehydration within this mantle wedge could induce the upwelling of deep-seated hot material [7] (Figure 8). Concurrently, the collision between the Indian Ocean and Asian plates likely induced lateral compression of the mantle asthenosphere, possibly enhancing upwelling beneath the North China Craton and the Hubao Basin [8]. Since the Eocene epoch, the activity of the Daqing Mountain Frontal Fault has been notable, influenced by distant effects from the collision between India and Eurasia, alongside shifts in Pacific plate motion [58]. The presence of deep faults could facilitate deep heat convection, contributing to geothermal anomalies observed in the Hubao Basin.

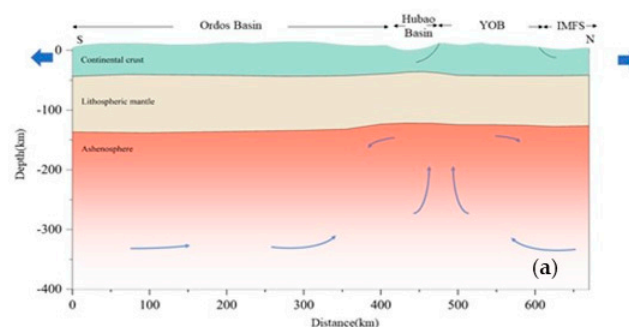
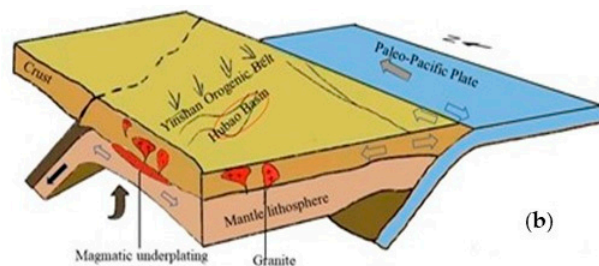


Figure 8. Cont.



**Figure 8.** Schematic diagram of the structural genesis mechanism in the Hubao Basin ((a) is the two-dimensional mechanism diagram, arrows represent the upwelling from the hot upper mantle pushing the lower, and (b) is the three-dimensional mechanism diagram, the arrows represent the interactions between and within plates).

## 6. Conclusions

Based on temperature measurement data and rock thermal conductivity data, this study calculated the geothermal gradient and terrestrial heat flow of the Hubao Basin. Subsequently, combined with the Yanchuan–Baotou–Mandula geophysical profile, the thermal structure of the lithosphere and the deep geodynamic mechanism of the Hubao Basin were investigated. The following conclusions were drawn:

1. The thermal conductivity of the Hubao Basin ranges from 1.83 to 5.35 W/(m·K), with the geothermal gradient ranging from 10.2 to 33.9 °C/km. The terrestrial heat flow values range from 64.0 to 73.8 mW/m<sup>2</sup>, with an average of  $65.7 \pm 14.7$  mW/m<sup>2</sup>, surpassing the mainland China average of  $60.4 \pm 12.3$  mW/m<sup>2</sup>.
2. Along the geophysical profile, the thermal condition of the lithosphere exhibits significant heterogeneity. The Moho temperature ranges from 570 to 652 °C, and the thickness of the thermal lithosphere shows a trend from thick to thin and then thick again from the Ordos Basin to the Hubao Basin and further to the Inner Mongolia Fold System. The average thickness of the thermal lithosphere is approximately 135.1 ± 4.02 km for the Ordos Basin, 122.9 ± 0.21 km for the Hubao Basin, 125.4 ± 1.04 km for the Yinshan Orogenic Belt, and 128.1 ± 0.45 km for the Inner Mongolia Fold System.
3. The formation and evolution of the Hubao Basin are influenced by the collision between the Indian Plate and the Eurasian Continent, as well as the westward subduction of the Pacific Plate. The Ural Mountains and Daqing Mountains Frontal Faults within the basin, with significant segmentation, serve as potential channels for thermal anomalies.

**Author Contributions:** Investigation, G.Z. and T.G.; software, Y.Y.; supervision, S.W.; writing—original draft, Z.G.; writing—review and editing, W.X., X.T. and G.Z. All authors discussed the basic structure of the manuscript. All authors have read and agreed to the published version of the manuscript.

**Funding:** This research was funded by the National Natural Science Foundation of China, grant number 42172335.

**Data Availability Statement:** The data that support the findings of this study are available from the corresponding author (Wei Xu) upon reasonable request.

**Acknowledgments:** Our heartfelt gratitude is given to the editor and the reviewers for their scientific and linguistic revisions of the manuscript.

**Conflicts of Interest:** Author Gengeng Zhu was employed by the company Exploration and Development Institute of PetroChina Changqing Oilfield Company. The remaining authors declare that the research was conducted in the absence of any commercial or financial relationships that could be construed as a potential conflict of interest.

## References

1. Wang, J.Y.; Zhang, J.; Xu, H.H.; Hu, S.B.; Huang, S.P.; Shi, X.B.; Yang, X.Q.; Shi, H.C.; Guo, X.W.; Liu, S.W.; et al. *Geothermal Science and Its Applications*, 1st ed.; Science Press: Beijing, China, 2015; pp. 1–548. (In Chinese)
2. Chen, X.B.; Zang, S.X.; Liu, Y.G.; Wei, R.Q. The current horizontal movement state of the Ordos block and its interaction with surrounding blocks. *J. Univ. Chin. Acad. Sci.* **2005**, *3*, 309–314.
3. Wang, T.; Xu, M.J.; Wang, L.S.; Liu, S.W.; Hu, X.Z. The characteristics of aeromagnetic anomalies in Ordos and its adjacent areas and their tectonic significance. *Chin. J. Geophys.* **2007**, *1*, 163–170.
4. Wang, Q.S.; Teng, J.W.; Wang, G.J.; Xu, Y. Special regional gravity and magnetic fields and deep structures in the Yinshan area of Inner Mongolia. *Chin. J. Geophys.* **2005**, *2*, 314–320.
5. Xu, L.B.; Wei, W.B.; Jin, S.; Ye, G.F.; Liang, H.D.; Jia, C.X.; Gong, X.; Yu, Y. Research on the deep electrical structural characteristics of the northern part of the Ordos block to the Yinshan orogenic belt. *Chin. J. Geophys.* **2017**, *60*, 575–584.
6. Feng, S.Y.; Liu, B.J.; Ji, J.F.; He, Y.J.; Tan, Y.L.; Li, Y.Q. Deep seismic reflection detection of the fine structure of the lithosphere in the Hohhot Baotou Basin. *Chin. J. Geophys.* **2015**, *58*, 1158–1168. [[CrossRef](#)]
7. Tian, X.B.; Teng, J.W.; Zhang, H.S.; Zhang, Z.J.; Zhang, Y.Q.; Yang, H.; Zhang, K.K. Structure of crust and upper mantle beneath the Ordos Block and the Yinshan Mountains revealed by receiver function analysis. *Phys. Earth Planet. Inter.* **2011**, *184*, 186–193. [[CrossRef](#)]
8. Liu, M.; Cui, X.J.; Liu, F.T. Cenozoic rifting and volcanism in eastern China: A mantle dynamic link to the Indo-Asian collision? *Tectonophysics* **2004**, *393*, 29–42. [[CrossRef](#)]
9. Teng, J.W.; Wang, F.Y.; Zhao, W.Z.; Zhang, Y.Q.; Zhang, X.K.; Yan, Y.F.; Zhao, J.R.; Li, M.; Yang, H.; Zhang, H.S.; et al. The Yinshan Orogenic Belt—Ordos Basin Rock Sphere, Block Velocity Structure, and Deep Dynamic Processes. *Chin. J. Geophys.* **2010**, *53*, 67–85.
10. Zhang, Y.Q.; Teng, J.W.; Wang, F.Y.; Zhao, W.Z.; Li, M.; Wang, Q.S. The seismic wave attribute structure and lithology inference of the upper crust in the Yinshan orogenic belt and the northern region of the Ordos Basin. *Chin. J. Geophys.* **2011**, *54*, 87–97.
11. Afonso, C.J.; Fernández, M.; Ranalli, G.; Griffin, W.L.; Connolly, J.A.D. Integrated geophysical-petrological modeling of the lithosphere and sublithospheric upper mantle: Methodology and applications. *Geochem. Geophys. Geosyst.* **2008**, *9*. [[CrossRef](#)]
12. Li, J.; Han, X.M.; Wang, X.S.; Yang, H.Y.; Zhang, F.; Zhang, H. Analysis of the stress field state of the seismic source in the Hohhot Baotou Basin. *Seismol. Geomagn. Obs. Res.* **2017**, *38*, 57–64.
13. Dong, T. Structural Composition and Formation and Evolution Process of the Western Section of the Northern Margin Fault Zone of the North China Craton, China. Master's Thesis, China University of Geosciences (Beijing), Beijing, China, 2021; pp. 1–54.
14. Shao, J.A.; Mu, B.L.; He, G.Q.; Zhang, L.Q. Geological processes in the tectonic superposition process of the ancient Asian and Pacific domains in northern North China. *Sci. Sin.* **1997**, *27*, 390–394.
15. Zhang, C. Rock Assemblages, Zircon U-Pb Geochronological Characteristics, and Geological Significance of the Bainaimiao Group in the Sunite Right Banner Area of Inner Mongolia, China. Master's Thesis, Jilin University, Jinlin, China, 2013; pp. 1–68.
16. Wang, X.L. Research on Quaternary Sedimentary and Structural Characteristics of the Hubao Basin in Inner Mongolia, China. Master's Thesis, China University of Geosciences (Beijing), Beijing, China, 2007; pp. 1–68.
17. Geological Survey and Research Institute of Jilin University. *Regional Geological Survey Report Baotou City Range (K49C004002)*; Geological Survey and Research Institute of Jilin University: Changchun, China, 2005; Available online: [http://www.ngac.org.cn/Data/archivesFileBrowsing?DocId=cgdoi.n0001/d00122694.z01\\_0002](http://www.ngac.org.cn/Data/archivesFileBrowsing?DocId=cgdoi.n0001/d00122694.z01_0002) (accessed on 10 August 2023).
18. Xu, X.W.; Cheng, G.L.; Ma, X.Y.; Sun, Y.H.; Han, Z.J. The rotational patterns and power sources of North China and its neighboring blocks. *Earth Sci.* **1994**, *19*, 129–138.
19. Deng, Q.D.; Cheng, S.P.; Min, W.; Yang, G.Z.; Ren, D.W. Discussion on the Cenozoic tectonic activity and dynamics of the Ordos block. *J. Geomech.* **1999**, *3*, 12–21.
20. Xu, W.; Li, Y.; Zhou, L.M.; Ke, T.T.; Cheng, L.Y. Lithospheric thermal regime under the Qinling Orogenic Belt and the Weihe Basin: A transect across the Yangtze and the North China cratons in central China. *Tectonophysics* **2020**, *789*, 228514. [[CrossRef](#)]
21. The Research Group of the Ordos Peripheral Active Fault System by the National Seismological Bureau. *The Ordos Peripheral Active Fault System*; Seismic Press: Beijing, China, 1988.
22. Xu, M.L.; Yang, Y.B.; Sun, C.Y.; Deng, Y.M.; Zhang, G.Z.; Shi, S.L.; Su, Z.N.; Feng, C.H. Geophysical response and analysis of controlling structures for sandstone type uranium deposits in the northern Ordos Basin. *Geol. Rev.* **2023**, *69*, 213–214. [[CrossRef](#)]
23. Chen, L. Concordant structural variations from the surface to the base of the upper mantle in the North China Craton and its tectonic implications. *Lithos* **2010**, *120*, 96–115. [[CrossRef](#)]
24. Zhao, G.C.; Wilde, S.A.; Cawood, P.A.; Sun, M. Archean blocks and their boundaries in the North China Craton: Lithological, geochemical, structural and path constraints and tectonic evolution. *Precambrian Res.* **2001**, *107*, 45–73. [[CrossRef](#)]
25. Bai, L.X. The Era Determination of the Latest Tectonic Movement in Daqingshan and Its Impact on the Tectonic Evolution of the Hetao Basin, China. Master's Thesis, Institute of Geology, China Earthquake Administration, Beijing, China, 2018; pp. 1–80.
26. Hu, J.; Tian, Y.T.; Li, Z.W.; Jiang, G.Z.; Zuo, Y.H.; Zhang, C.; Wang, Y.B.; Wang, Y.C.; Hu, S.B. GeothermoTool: An open-source software for basic geothermal calculations and plots. *Geothermics* **2022**, *106*, 102551. [[CrossRef](#)]
27. Jiang, G.Z.; Hu, S.B.; Shi, Y.Z.; Zhang, C.; Wang, Z.T.; Hu, D. Terrestrial heat flow of continental China: Updated dataset and tectonic implications. *Tectonophysics* **2019**, *753*, 36–48. [[CrossRef](#)]

28. Hu, S.B.; He, L.J.; Wang, J.Y. Heat flow in the continental area of China a new data set. *Earth Planet. Sci. Lett.* **2000**, *179*, 407–419. [[CrossRef](#)]
29. Zhang, Q.R.; Xiao, H.P.; Rao, S.; Shi, Y.Z.; Li, W.J.; Huang, S.D.; Hu, G.M. The characteristics and controlling factors of the current geothermal field in the Songliao Basin. *Bull. Geol. Sci. Technol.* **2023**, *42*, 191–204. [[CrossRef](#)]
30. Zeyen, H.; Fernández, M. Integrated Lithospheric Modeling Combining Thermal, Gravity, and Local Isostasy Analysis—Application to the Ne Spanish Geotranssect. *J. Geophys. Res.-Solid Earth* **1994**, *99*, 18089–18102. [[CrossRef](#)]
31. Ricard, Y. Mantle convection in the Earth and planets. *Science* **2002**, *295*, 802–803. [[CrossRef](#)]
32. Connolly, J.A.D. Computation of phase equilibria by linear programming: A tool for geodynamic modeling and its application to subduction zone decarbonation. *Earth Planet. Sci. Lett.* **2005**, *236*, 524–541. [[CrossRef](#)]
33. Carballo, A.; Fernandez, M.; Jimenez-Munt, I.; Torne, M.; Vergés, J.; Melchiorre, M.; Pedreira, D.; Afonso, J.C.; Garcia-Castellanos, D.; Díaz, J.; et al. From the North-Iberian Margin to the Alboran Basin: A lithosphere geo-transect across the Iberian Plate. *Tectonophysics* **2015**, *663*, 399–418. [[CrossRef](#)]
34. Wang, Q.S.; Teng, J.W.; An, Y.L.; Zhang, Y.Q. Gravity Field and Deep Structures in the Yinshan Mountains and the Northern Ordos Basin. *Prog. Geophys.* **2010**, *25*, 1590–1598.
35. Jiang, G.Z.; Gao, P.; Rao, S.; Zhang, L.Y.; Tang, X.Y.; Huang, F.; Zhao, P.; Pang, Z.H.; He, L.J.; Hu, S.B.; et al. Compilation of terrestrial heat flow data in Chinese Mainland (fourth edition). *Chin. J. Geophys.* **2016**, *59*, 2892–2910.
36. Ma, X.Y.; Liu, C.S.; Liu, G.D. The geological section from Xiangshui, Jiangsu to Mandula, Inner Mongolia. *Acta Geol. Sin.* **1991**, *3*, 199–215. [[CrossRef](#)]
37. Pavlis, N.K.; Holmes, S.A.; Kenyon, S.C.; Factor, J.K. The development and evaluation of the Earth Gravitational Model 2008 (EGM2008). *J. Geophys. Res. Solid Earth* **2012**, *117*. [[CrossRef](#)]
38. Sandwell, D.T.; Harper, H.; Tozer, B.; Smith, W.H.F. Gravity field recovery from geodetic altimeter missions. *Adv. Space Res.* **2021**, *68*, 1059–1072. [[CrossRef](#)]
39. Chen, Z.Y. Geological and Tectonic Evolution of the Middle Proterozoic Paleozoic in the Guyang Mandula Region of Inner Mongolia, China. Doctoral Thesis, China University of Geosciences (Beijing), Beijing, China, 2005; pp. 1–151.
40. Ran, Y.K.; Zhang, P.Z.; Chen, L.C. Research on the Late Quaternary Paleoseismic Integrity of the Daqing Mountain Front Fault in the Hetao Fault Zone. *Earth Sci. Front.* **2003**, *51*, 207–216.
41. Li, M.K.; Song, X.D.; Li, J.T.; Bao, X.W. Lithospheric structure and tectonic significance of large basins in Chinese Mainland. *Earth Sci.* **2018**, *43*, 3362–3372.
42. Artemieva, I.M.; Mooney, W.D. The continental lithosphere: Reconciling thermal, seismic, and petrologic data. *Lithos* **2009**, *109*, 23–46. [[CrossRef](#)]
43. Huang, F.; He, L.J.; Wu, Q.J. Lithospheric thermal structure of the Ordos Basin and its implications to destruction of the North China Craton. *Chin. J. Geophys.* **2015**, *58*, 3671–3686.
44. Zang, S.X.; Liu, Y.G.; Ning, J.Y. Thermal structure of lithosphere in North China. *Chin. J. Geophys.* **2002**, *45*, 51–62.
45. Rao, S.; Jiang, G.Z.; Gao, Y.J.; Hu, S.B.; Wang, J.Y. The thermal structure of the lithosphere and heat source mechanism of geothermal field in Weihe Basin. *Chin. J. Geophys.* **2016**, *59*, 2176–2190.
46. Zuo, Y.H.; Jiang, S.; Wu, S.H.; Xu, W.; Zhang, J.; Feng, R.P.; Yang, M.H.; Zhou, Y.S.; Madhava, S. Terrestrial heat flow and lithospheric thermal structure in the Chagan Depression of the Yingen-Ejinaqi Basin, north central China. *Basin Res.* **2020**, *32*, 1328–1346. [[CrossRef](#)]
47. Qiu, N.S.; Zuo, Y.H.; Chang, J.; Xu, W.; Zhu, C.Q. Comparison of Mesozoic and Cenozoic thermal systems in typical basins of eastern and western China. *Earth Sci. Front.* **2015**, *22*, 157–168. [[CrossRef](#)]
48. Zuo, Y.H.; Qiu, N.S.; Chang, J.; Hao, Q.Q.; Li, Z.X.; Li, J.W.; Li, W.Z.; Xie, C.H. Research on the thermal structure of the Mesozoic and Cenozoic lithosphere in the Bohai Bay Basin. *Acta Geol. Sin.* **2013**, *87*, 145–153.
49. Xu, W. Research on the Mesozoic Cenozoic Thermal System and Lithospheric Thinning in the Bohai Bay Basin, China. Doctoral Thesis, China University of Petroleum (Beijing), Beijing, China, 2019; pp. 1–109.
50. Liu, S.W.; Li, X.L.; Hao, C.Y.; Li, X.D. Heat flow, deep temperature and thermal structure in Tarim Basin. *Earth Sci. Front.* **2017**, *24*, 41–55. [[CrossRef](#)]
51. Liang, Y.B. The first discovery of uranium thorium ore and cerium sodium carbonate ore in the Baiyun Ebo iron mining area. *Geol. Explor.* **1979**, *8*, 21.
52. Yang, M.Z.; Li, Y.C. Research on uranium thorium minerals in the Baiyun Ebo deposit in Inner Mongolia. *China Sci. Bull.* **1980**, *12*, 558–560.
53. Zhao, C.Y. Thorium and Uranium in Baiyun Ebo (1). *Rare Earth Inf.* **2006**, *7*, 12–15.
54. Wang, X.K. Geochemical Evaluation of Urban Ecosystems in Hohhot and Baotou Cities, China. Doctoral Thesis, China University of Geosciences (Beijing), Beijing, China, 2012; pp. 1–150.
55. Wang, P.J.; Li, X.L.; Gong, Y.L.; Li, B.H.; Zhang, X. Using aerial geophysical data to delineate hidden rock (magnetic) bodies—taking the Bayannur Baotou area as an example. *Geol. Chem. Miner.* **2012**, *34*, 249–254.
56. Lei, J.S.; Zhai, D.P. P-wave tomography and origin of the Changbai intraplate volcano in Northeast Asia. *Tectonophysics* **2005**, *397*, 281–295. [[CrossRef](#)]

57. Zhao, D.P.; Maruyama, S.; Omori, S. Mantle dynamics of Western Pacific and East Asia: Insight from seismic tomography and mineral physics. *Gondwana Res.* **2007**, *11*, 120–131. [[CrossRef](#)]
58. Zhang, J.J.; Zheng, J.L.; Wang, H.B.; Guo, L.; Liu, J.; Qi, G.W. The Late Mesozoic Early Cenozoic tectonic events in Daqingshan Panyangshan, Inner Mongolia and their implications for the tectonic evolution of the northern margin of North China. *Earth Sci. Front.* **2024**, *31*, 127–141. [[CrossRef](#)]

**Disclaimer/Publisher's Note:** The statements, opinions and data contained in all publications are solely those of the individual author(s) and contributor(s) and not of MDPI and/or the editor(s). MDPI and/or the editor(s) disclaim responsibility for any injury to people or property resulting from any ideas, methods, instructions or products referred to in the content.